Mathematical Modeling of Preclinical Alpha-Emitter Radiopharmaceutical Therapy

Alireza Karimian[1], Nathan T. Ji[2], Hong Song[2], and George Sgouros[2]

ABSTRACT

Preclinical studies, *in vivo*, and *in vitro* studies, in combination with mathematical modeling can help optimize and guide the design of clinical trials. The design and optimization of alpha-particle emitter radiopharmaceutical therapy (αRPT) is especially important as αRPT has the potential for high efficacy but also high toxicity. We have developed a mathematical model that may be used to identify trial design parameters that will have the greatest impact on outcome. The model combines Gompertzian tumor growth with antibody-mediated pharmacokinetics and radiation-induced cell killing. It was validated using preclinical experimental data of antibody-mediated ^{213}Bi and ^{225}Ac delivery in a metastatic transgenic breast cancer model. In modeling simulations, tumor cell doubling time, administered antibody, antibody specific-activity, and antigen-site density most impacted median survival. The model was also used to investigate treatment fractionation. Depending upon the time-interval between injections, increasing the number of injections increased survival time. For example, two administrations of 200 nCi, ^{225}Ac-labeled antibody, separated by 30 days, resulted in a simulated 31% increase in median survival over a single 400 nCi administration. If the time interval was 7 days or less, however, there was no improvement in survival; a one-day interval between injections led to a 10% reduction in median survival. Further model development and validation including the incorporation of normal tissue toxicity is necessary to properly balance efficacy with toxicity. The current model is, however, useful in helping understand preclinical results and in guiding preclinical and clinical trial design towards approaches that have the greatest likelihood of success.

Significance: Modeling is used to optimize αRPT.

Introduction

Radiopharmaceutical therapy (RPT) entails the delivery of radiation to tumor cells by means of systemically administered radiolabeled carriers that are engineered to target specific tumor-associated markers or that accumulate in tumors or the tumor microenvironment due to physiologic processes. Examples of the former include radiolabeled antibodies (1), peptides (2), and small molecules (3). Examples of the latter include yttrium-90-labeled microsphere therapy of hepatic cancer (4), radioiodine therapy of thyroid cancer (5), and radium-223-dichloride (Xofigo) therapy of skeletal metastases (6). In particular, the use of radionuclides that emit alpha-particles has highlighted the unique ability of RPT to deliver highly potent, alpha-particle radiation to widely disseminated metastatic cancer. The pattern of radiation damage associated with alpha-particle tracks leads to DNA damage that is predominantly in the form of double-stranded breaks (7). Such damage is less easily repaired and cellular lethality can be achieved without the need to accumulate a large number of DNA-damaging events. Accordingly, alpha-particle induced tumor cell lethality is not susceptible to most resistance mechanism, including oxygenation status, cell-signaling pathway redundancy, and drug effusion pumps. Tumor cells that have shown resistance to photon radiotherapy are not resistant to alpha-particles (8, 9). In human studies, α-emitters have yielded significant survival results in adult leukemia (10, 11), glioblastoma multiforme (12), and hormone-refractory metastatic prostate cancer (13–15), all cancers for which there are few to no treatment options. The design and optimization of alpha-particle emitter RPT (αRPT) is especially important as αRPT has the potential for high efficacy but also high toxicity. Furthermore, because αRPT is likely to be most effective in targeting metastatic disease, the evaluation of such trials is not amenable to standard imaging-based criteria such as "RECIST" (16) or "PET Response Criteria In Solid Tumors" (PERCIST; ref. 17).

The mechanism by which radiation kills cells is generally well understood and has been modeled, both *in vitro* and *in vivo* (18–21). We have combined modeling of radiation-induced cell killing with a model of antibody–antigen binding and dissociation and also with Gompertzian modeling of cellular proliferation to fit preclinical therapeutic studies of alpha-emitter antibody-mediated RPT in a disseminated breast cancer model (22). The alpha-emitters, actinium-225 (10-day half-life, 4 α-particles emitted in the decay chain) and bismuth-213 (45.6-minute half-life, 1 α-particle emitted) were used with an antibody against the rat analog of HER2/*neu* in a transgenic, immune-intact mouse model. The simulations have been used to identify those variables that are critical to the success of antibody-mediated RPT in targeting widespread, rapidly accessible metastatic cancer with these two alpha-emitters. The focus of the modeling simulations is on ^{225}Ac because this alpha-emitter is of greater preclinical and clinical interest. The ^{213}Bi studies are included for model validation.

[1]Department of Biomedical Engineering, Faculty of Engineering, University of Isfahan, Isfahan, Iran. [2]Radiologic Physics Division, Russell H. Morgan Department of Radiology and Radiological Science, Johns Hopkins University, School of Medicine, Baltimore, Maryland.

Note: Supplementary data for this article are available at Cancer Research Online (http://cancerres.aacrjournals.org/).

A. Karimian and N.T. Ji contributed equally to this article.

Current address for H. Song: Department of Radiology, School of Medicine, Stanford University, Stanford, California.

Corresponding Author: George Sgouros, Johns Hopkins University School of Medicine, 1550 Orleans St., 4M61 CRB II, Baltimore, MD 21287. Phone: 410-614-0116; Fax: 413-487-3753; E-mail: gsgouros@jhmi.edu

Cancer Res 2020;80:868–76

doi: 10.1158/0008-5472.CAN-19-2553

Materials and Methods

^{225}Ac-7.16.4 survival studies

Survival data from preclinical studies investigating the therapeutic efficacy and toxicity of ^{213}Bi- and ^{225}Ac-labeled anti-*neu* antibody in a transgenic murine model of metastatic breast cancer were used for model development and validation. The transgenic murine model (23) and ^{213}Bi studies were reported previously (24). Details regarding the anti-HER2/neu antibody, 7.16.4 are described in ref. 22 and briefly summarized below. In addition, previously unpublished, survival studies of mice treated with ^{225}Ac-labeled 7.16.4 antibody following left cardiac ventricle (LCV) tumor cell injection that we have used for model validation are described herein.

neu-N transgenic mice, age 6 to 8 weeks, expressing rat HER-2/*neu* under the mouse mammary tumor virus (MMTV) promoter were obtained from Harlan (Harlan Laboratory). All experiments involving the use of mice were conducted with the approval of the Animal Care and Use Committee of The Johns Hopkins University School of Medicine. NT2.5, a rat HER-2/*neu* expressing mouse mammary tumor cell line, was established from spontaneous mammary tumors and authenticated as described previously (25). The NT2.5 cells were maintained in RPMI media containing 20% FBS, 0.5% penicillin/streptomycin (Invitrogen), 1% L-glutamine, 1% nonessential amino acids, 1% sodium pyruvate, 0.02% gentamicin, and 0.2% insulin (Sigma) at 37°C in 5% CO_2. 7.16.4, a mouse anti-rat HER-2/*neu* mAb was purified from the ascites of athymic mice. The hybridoma cell line was kindly provided by Dr. Mark Greene (University of Pennsylvania, Philadelphia, PA).

Radiolabeling of antibody with ^{225}Ac

7.16.4 was conjugated to SCN-CHX-A"-DTPA following a previously published protocol (26).

^{225}Ac was purchased from Curative Technologies Corporation. ^{225}Ac was labeled to mAb in a two-step reaction following McDevitt and colleagues (27). First, ^{225}Ac (0.15–0.2 mCi in 20–80 μL) was chelated to 1 μL (10 mg/mL) *p*-SCN-Bn-DOTA (Macrocyclics) at 56°C for 1 hour. Ascorbic acid (1 μL, 150 mg/mL) was added as a radioprotectant and 2M sodium acetate (40–60 μL) was added to raise the pH to 6.5. The efficiency of ^{225}Ac chelation to DOTA was determined by Sephadex C-25 column (GE Bioscience). Second, 100 μg mAb (~20 μL, 5 mg/mL) was incubated with *p*-SCN-Bn-DOTA-^{225}Ac at 37°C for 45 minutes (pH 8.5). ^{225}Ac-labeled mAb was purified with a Centricon centrifuge filter unit (YM-10; Millipore).

The reaction efficiency and purity of the radioimmunoconjugate was determined with instant thin layer chromatography (ITLC) using silica gel impregnated paper (Gelman Science Inc.). ITLC paper strips were counted the next day with a gamma counter (LKB Wallac; Perkin-Elmer) to allow ^{225}Ac to reach equilibrium. ^{225}Ac-7.16.4 immunoreactivity was determined by incubating 5 ng of ^{225}Ac-7.16.4 with excess antigen binding sites (1×10^7 NT2.5 cells) twice on ice for 30 minutes each time. Immunoreactivity was calculated as the percentage of ^{225}Ac-7.16.4 bound to the cells. Stability of ^{225}Ac-7.16.4 was measured by incubating ^{225}Ac-7.16.4 in cell culture media containing 20% FBS for 30 days and the fraction of ^{225}Ac chelated to DOTA was measured with Sephadex C-25 column and ITLC.

Three days after *neu*-N mice were injected with 1×10^5 NT2.5 cells into the LCV, mice were treated intravenously with 400 ($n = 5$) or 300 ($n = 7$) nCi ^{225}Ac-7.16.4; untreated mice ($n = 7$) served as controls. Mice were observed and weighed three times per week and were euthanized if significant body weight loss (>15%) or hind limb paralysis appeared.

Model description

The *in silico* model developed to fit preclinical ^{213}Bi and ^{225}Ac-7.16.4 survival study data is depicted in **Fig. 1** and described by Equations A–P.

$$\frac{d}{dt}N_c = (\gamma - \delta)N_c - (k_+ \cdot \mathrm{Ab})N_c + k_- \cdot N_h \quad \text{(A)}$$

$$\frac{d}{dt}N_h = (\gamma - (\delta + \kappa))N_h - k_- \cdot N_h + (k_+ \cdot \mathrm{Ab})N_c \quad \text{(B)}$$

$$\frac{d}{dt}\mathrm{Ab} = s(k_- \cdot N_h - k_+ \cdot N_c)\mathrm{Ab} - \lambda_{bio} \cdot \mathrm{Ab} \quad \text{(C)}$$

$$\gamma = \frac{\ln(2)}{T_d}, \quad \text{growth rate } \left(h^{-1}\right) \quad \text{(D)}$$

$$\delta = \gamma\varphi(N), \quad \text{cell loss rate } \left(h^{-1}\right) \quad \text{(E)}$$

$$\varphi(N) = \frac{\ln\left(\frac{N}{N_0}\right)}{\ln\left(\frac{N_\infty}{N_0}\right)}, \quad \text{cell loss factor} \quad \text{(F)}$$

$$s = \frac{Ag_0}{6.023 \times 10^{14}}, \quad \text{nmoles of antigen per cell (nmol)} \quad \text{(G)}$$

$$\lambda = \frac{\ln(2)}{T_{1/2}}, \quad \text{decay rate of the radionuclide } \left(h^{-1}\right) \quad \text{(H)}$$

$$\sigma(t) = \sigma_0' e^{-\lambda(t)}, \quad \text{specific activity (Bq/nmol)} \quad \text{(I)}$$

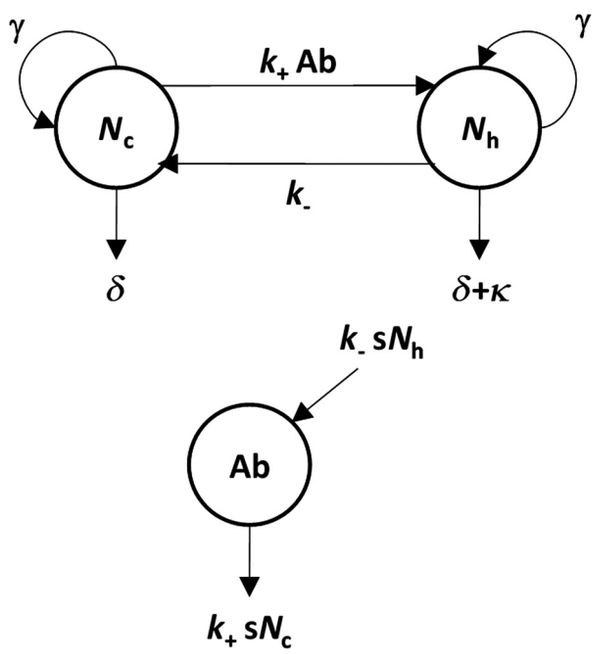

Figure 1.
Depiction of mathematical model used to simulate targeted alpha-emitter therapy. The model describes the evolution of tumor burden ($N = N_h + N_c$) and antibody (Ab) available for tumor–cell binding over time.

$$\sigma_0^{'} = \sigma_0 e^{\lambda T_{\text{inj}}}, \quad \text{initial specific activity (Bq/nmol), at inj. time, } T_{\text{inj}}, \tag{J}$$

$$\lambda_{\text{bio}} = \frac{\ln(2)}{T_{\text{bio}}}, \quad \text{Ab loss due to biological clearance } \left(h^{-1}\right) \tag{K}$$

$$\kappa = a \cdot d \cdot e, \quad \text{cell kill rate } \left(h^{-1}\right) \tag{L}$$

$$a = \left(\frac{1}{2}\right)^{\frac{t-T_{\text{inj}}}{T_d}} \cdot s \cdot \sigma(t), \quad \text{radioactivity per cell (Bq)} \tag{M}$$

$$d = S(n, cs) \cdot 3600, \text{cellular s-factor, absorbed dose rate to cell nucleus per activity on cell surface (Gy/h/Bq)} \tag{N}$$

$$e = \frac{1}{D_0}, \quad \text{cell kill rate per unit absorbed dose } (Gy^{-1}) \tag{O}$$

$$N = N_h + N_c, \quad \text{total number of tumor cells} \tag{P}$$

where N_h is the radiolabeled (hot) cells; N_c the nonradioactive (cold) cells; Ab the unbound (free) radiolabeled antibody (nmol); D_0 the cell radiosensitvity (Gy); T_d the tumor cell doubling time (hours); Ab_0 the administered radiolabeled antibody (nmol); N_0 the initial number of tumor cells; N_∞ the maximum number of tumor cells; Ag_0 the antigen sites per cell; k_+ the Ab–Ag association rate ($nmol^{-1}$ h^{-1}); k_- the Ab–Ag dissociation rate (h^{-1}); σ_0 the initial specific activity (Bq/nmol); T_{inj} the time interval between tumor cell inoculation and antibody injection (hours); $T_{1/2}$ the radionuclide half-life (hours); T_{bio} is the biological clearance half-life of Ab (hours).

The model applies to cells distributed throughout the vascular volume that are rapidly accessible to intravenously-administered radiolabeled antibody. Tumor cells in this volume are characterized by their radiosensitivity (D_0), doubling time (T_d) and initial cell-surface antigen density (Ag_0). In initial model simulations all cells were assigned a single value rather than sampling from a distribution of values for each parameter. Equations A and B describe the transition of cells from their initial, radiolabeled antibody-free "cold" state to the radiolabeled antibody-bound "hot" state. The transition is governed by the number of antigen sites available for binding, the amount of available antibody in the vascular volume and the antibody–antigen binding and dissociation rates, k_+ and k_-, respectively. "Cold" cells (N_c) become "hot" (N_h) at a rate proportional to the free Ab available. Reduction in N_h occurs due to Ab dissociation at rate, k_-, cell loss due to cell turnover, δ, or elimination by radiation-induced cell kill (κ). Loss via Ab dissociation returns N_h to N_c, whereas loss due to turnover or cell kill removes the cells from the model. Loss due to radiation induced cell kill only operates on hot cells. Loss due to "turnover" occurs on both N_h and N_c. This loss rate is proportional to the total number of cells in the vascular volume of the mouse. The initial exponential growth rate of N_c and N_h, is γ. Consistent with Gompertzian tumor growth kinetics, the growth rate is reduced as $N_c + N_h$, increase (28). When $\delta + \kappa > \gamma - k_-$, there is a net reduction in N_h. If $\gamma - k_- > \delta + \kappa$, then cells have an opportunity to escape kill by Ab dissociation.

Equation C describes the antibody available for tumor cell antigen binding. The level of free antibody is governed by binding to and dissociation from antigen sites (first term of Eq. C) and by biological clearance from the vascular volume (second term of Eq. C). Available Ab for transferring N_c to N_h is reduced at a rate proportional to the product of the number of N_c and the number of sites per cell, s. Dissociation of Ab from hot cells replenishes Ab at a rate proportional to the product of N_h and s.

The amount of radioactivity available for cell binding is determined by the specific activity of the antibody [$\sigma(t)$]. The time-dependence of the specific activity reflects physical decay of the radionuclide. The impact of cell division and resulting dilution of the activity per cell was incorporated by assuming that the activity per cell is halved after each division (Eq. M). This approach reduces the activity per cell and, therefore, the kill-rate but does not return N_h to N_c.

To avoid increasing model complexity, internalization has not been incorporated into the current version of the model. If warranted, this could be included by introducing a third compartment to which N_h may enter at a rate consistent with Ab internalization.

The system of differential equations describing this model were solved numerically using MATLAB R2018b.

Simulations and parameter values to fit experimental data

The model was validated by comparing simulated results to survival data from the preclinical studies. The parameters used to fit each

Table 1. Parameter values for each simulation.

	Simulation number						
Parameter	**1**	**2**	**3**	**4**	**5**	**6**	**7**
Radionuclide	—	—	^{213}Bi	^{213}Bi	^{213}Bi	^{225}Ac	^{225}Ac
Admin. activity	—	—	4.4 MBq (120 μCi)	3.3 MBq (90 μCi)	4.4 MBq (120 μCi)	14.8 kBq (400 nCi)	11.1 kBq (300 nCi)
N_0	10^5	10^4	10^5	10^5	10^4	10^5	10^5
N_∞	2×10^8	2×10^8	2×10^8	2×10^8	2×10^8	2×10^8	2×10^8
Ab_0 (μg)	—	—	10	10	10	4	3
Ag_0 (site/cell)	1×10^5	1×10^5	1×10^5	1×10^5	1×10^5	1×10^5	1×10^5
σ_0 (Bq/nmol)	—	—	2.2×10^7	1.7×10^7	2.2×10^7	5.6×10^5	4.2×10^5
k_+ ($nmol^{-1}$ h^{-1})	47.25	47.25	47.25	47.25	47.25	47.25	47.25
k_- ($hour^{-1}$)	0.001	0.001	0.001	0.001	0.001	0.001	0.001
T_{inj} (days)	—	—	3	3	3	3	3
$T_{1/2}$ (hours)	—	—	0.76	0.76	0.76	240	240
T_{bio} (hours)	63	63	63	63	63	63	63
D_0 (Gy)	0.2	0.2	0.2	0.2	0.2	0.2	0.2
T_d (h)	25.8	25.8	25.8	25.8	25.8	25.8	25.8
S(n,cs) (Gy/s/Bq)	—	—	0.0495	0.0495	0.0495	0.235	0.235

simulation to their respective preclinical data are summarized in **Table 1**.

The initial number of cells, N_0, corresponds to the number of tumor cells administered for each model simulation to match experimental procedures. N_∞, the theoretical maximum number of tumor cells is used as a parameter that describes asymptotic tumor cell growth in the Gompertzian growth expression and was set to 2×10^8. In simulations of untreated mice after a tumor growth period, the value of 1×10^8 was obtained as the number of tumor cells at the median survival time. This value may be thought of as the cell number threshold beyond which mice do not survive, and was used to determine the survival times in simulations of untreated, ^{213}Bi treated, and ^{225}Ac treated mice.

Like the initial number of cells, the amount of antibody administered, Ab_0, is chosen based on the experimental procedures. The number of antigen sites per cell, Ag_0, is set based on measurements obtained for the NT2.5 cell line (23). The initial specific activity, σ_0, is determined by the experimental conditions. It is calculated by dividing the administered activity (in Bq) by the protein amount of antibody administered (in nmole). The antibody–antigen association and dissociation rate constants, k_+ and k_-, respectively were adjusted to match the observed median survival results for each experiment. The K_D for NT2.5 cells was measured as 2.1 nmol/L (23). This is a value obtained once equilibrium is reached. It represents the concentration of antibody at which half the cell-surface antigen sites are bound. Under *in vitro*, equilibrium conditions where there is a large excess of free antibody, the K_D may also be derived as k_-/k_+. The rate constants used in the simulations give a K_D that is about 5 orders of magnitude lower than the value measured, *in vitro*. This could reflect an internalization process that is not specifically considered by the model or an indication that the equilibrium conditions do not apply in a dynamic *in vivo* situation.

The time between LCV injection of tumor cells and tail-vein injection of the alpha-emitter labeled antibody, T_{inj}, was set to 3 days for all simulations to match experimental conditions. The physical half-life of each radionuclide is designated by $T_{1/2}$ and is 45.6 minutes (0.76 hours) for ^{213}Bi and 10 days (240 hours) for ^{225}Ac. The biological clearance half-life of the antibody, T_{bio}, was adjusted to 63 hours to match the observed median survival results for each experiment. The radiosensitivity, D_0, of 0.2 Gy is consistent with values previously reported for breast cancer cell lines irradiated with an alpha-particle emitter (29).

Parameter sensitivity analysis

Model parameters that most influenced median survival time were identified by varying each parameter individually while keeping all other parameters constant at the baseline values listed on **Table 1**. The following parameters were doubled: initial specific activity (σ_0), the amount of antibody administered (Ab_0), the number of antigen sites per cell (Ag_0), the cell kill rate per unit absorbed dose (e), the tumor cell doubling time and its related dilution rate, antibody–antigen association and dissociation rates (k_+ and k_-) and the biologic half-life (T_{bio}).

Treatment fractionation simulations

Fractionated administration of αRPT is already established clinically. The number of administrations and the time interval between them is usually chosen *ad hoc* or based on chemotherapy conventions. We examined the effect of different fractionation schedules on survival. Injection of 400 nCi ^{225}Ac was divided into two or four equal simulated injections. Different elapsed time intervals were also examined. Fractionation of treatment into four doses of 100 nCi was simulated with time intervals of 10, 15, 20, and 21 days.

In the fractionation simulations, we also examined the impact of selecting for a less sensitive or more rapidly growing cell population remaining after the first administration. This was accomplished by decreasing the tumor cell kill rate parameter, κ, and increasing the growth rate parameter, γ, respectively.

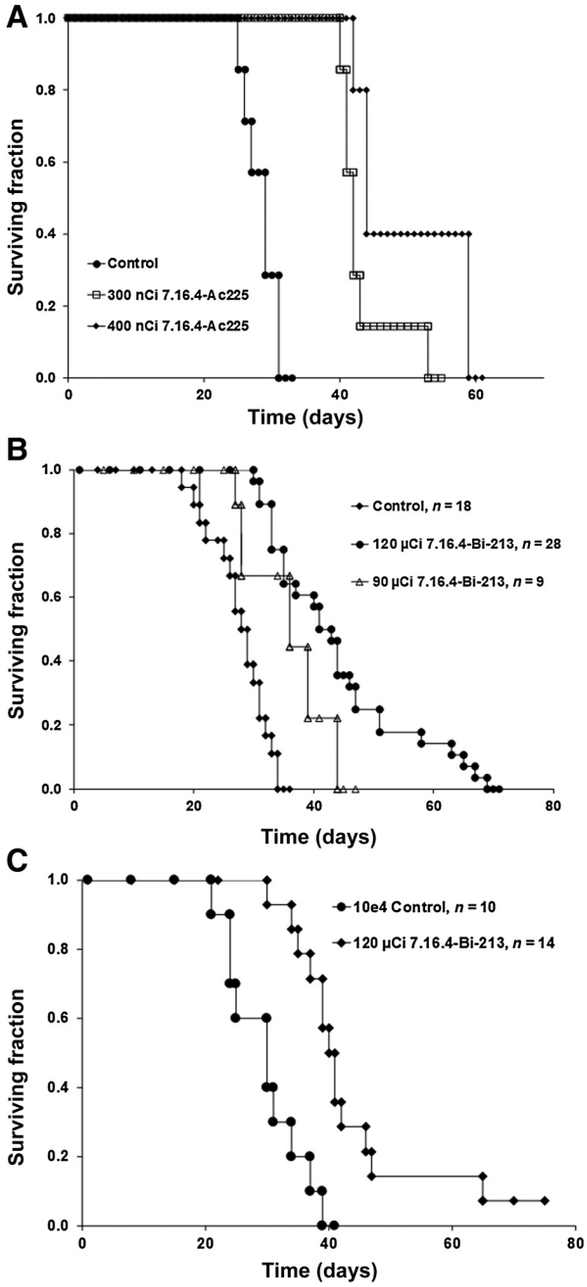

Figure 2.

Kaplan–Meier survival curves of neu-N transgenic mice treated at 3 days after LCV inoculation of 1×10^5 NT2.5 cells with 400 or 300 nCi ^{225}Ac-labeled 7.16.4 antibody (**A**). **B,** 1×10^5 NT2.5 cells with 90 or 120 µCi ^{213}Bi-labeled 7.16.4 (reproduced from **Fig. 3A** of ref. 24). **C,** 1×10^4 NT2.5 cells with 120 µCi of ^{213}Bi-7.16.4 (reproduced from **Fig. 4A** of ref. 24).

Table 2. Model validation; simulated versus measured results.

Initial no. of tumor cells	Radioisotope	Administered activity	Cohort size	Survival time		
				Experimental results (days)	Model-derived results (days)	Percent difference
1×10^4	Untreated	—	10[a]	30[a]	31.6	5.33
1×10^4	^{213}Bi	120 μCi	14[a]	41[a]	44.5	8.54
1×10^5	Untreated	—	18[a], 7[b]	28[a]	28.0	0.00
1×10^5	^{213}Bi	90 μCi	9[a]	36[a]	38.0	5.56
1×10^5	^{213}Bi	120 μCi	28[a]	41[a]	41.2	0.49
1×10^5	^{225}Ac	300 nCi	7[b]	43[b]	43.0	0.00
1×10^5	^{225}Ac	400 nCi	5[b]	47[b]	47.8	1.70

[a]From ref. 24.
[b]From **Fig. 1A**.

Results

Experimental data

Figure 2A–C depicts survival curves for the ^{225}Ac-7.16.4 and ^{213}Bi-7.16.4 studies used in model development and validation. The survival studies for both agents were conducted at their respective maximum tolerated activities (400 nCi and 120 μCi for ^{225}Ac-7.16.4 and ^{213}Bi-7.16.4, respectively). The results shown in **Fig. 2B** and **C** have been reported previously (24). The median survival times in the ^{225}Ac-7.16.4 studies for the control, 300 and 400 nCi groups were 28, 43, and 47 days, respectively. The median survival times in the ^{213}Bi-7.16.4 studies for the control, 90 and 120 μCi ^{213}Bi-7.16.4 groups were 28, 36, and 41 days, respectively. Median survival relative to control was improved in mice injected with 10-fold less cells; median survival time was 31 days for untreated mice and 44 days following 120 μCi ^{213}Bi-7.16.4 antibody treatment.

Using the parameter values (simulations 1, 3, 4, 6, 7) in **Table 1**, corresponding simulations of tumor cell number as functions of time are shown in **Fig. 3A**. Total tumor cell number for all treatment groups rapidly decreases following injection on the third day, reaching nadir on day 6, after which growth follows Gompertzian growth kinetics. The predicted median survival times from these simulations, taken as the number of days required to reach 10^8 tumor cells, are 28, 39, 42, 43, and 48 days, respectively, for untreated, 90 μCi-, 120 μCi-^{213}Bi-7.16.4, 300-, and 400 nCi-^{225}Ac-7.16.4–treated groups. Corresponding simulations (simulations 2, 5) of tumor cell number as functions of time from the animal model of **Fig. 1** but with 10^4 rather than 10^5 LCV inoculated tumor cells are also shown (**Fig. 3B**). In these simulations, a similar pattern is observed. The untreated group follows Gompertzian growth and the tumor cell number for the ^{213}Bi-7.16.4–treated group decreases to a nadir on day 6. The experimental studies showed that untreated mice injected with 10-fold less cells had median survival time of 31 days; median survival was 44 days following 120 μCi ^{213}Bi-7.16.4 antibody treatment. The simulations yield similar results, as corresponding median survival times (i.e., time required to reach 10^8 cells) is 32 and 45 days, respectively. A comparison of experimental versus simulated results is provided on **Table 2**. As shown on **Table 2**, model fits to the experimental median survival results are within 10%.

Parameter sensitivity analysis

Model sensitivity to parameter values was assessed by performing simulations for the ^{213}Bi and ^{225}Ac treatment studies while each of the parameter listed on **Table 3** was increased by a factor of 2. The resulting percent change in median survival time compared with baseline simulated survival times was tabulated for ^{225}Ac and ^{213}Bi. The results for both radionuclides show that median survival is most sensitive to tumor doubling time. Tumor cells with a growth rate half of that used in the baseline simulations (i.e., tumor doubling time increased by a factor of 2), yield a survival time approximately 2.6 times the survival time obtained for the baseline simulation of the group inoculated with 10^5 tumor cells and treated with 400 nCi ^{225}Ac-7.16.4. The next four most impactful parameters relate to the amount of ^{225}Ac-7.16.4 that is delivered to tumor cells. These are doubling antibody administered without reducing the specific activity (Ab_0 and σ_0), keeping antibody

Table 3. Effect of changing the parameters on survival time relative to baseline simulations for each radionuclide–antibody conjugate.

Doubled parameter	^{225}Ac-7.16.4 simulations			^{213}Bi-7.16.4 simulations		
	Survival time (days)	Percentage increase in survival time	Rank	Survival time (days)	Percentage increase in survival time	Rank
Not changed (baseline conditions)	47.8	0.0	—	41.2	0.0	—
Tumor doubling time (T_d)	126	163.6	1	82.3	99.8	1
Administered activity at constant specific activity (Ab_0, σ_0)	68.1	42.5	2	55.1	33.7	2
Initial specific activity (σ_0)	67.2	40.6	3	53.0	28.6	3
Antigen sites/cell (Ag_0)	67.2	40.6	3	53.0	28.6	3
Cell kill per unit absorbed dose (e)	67.2	40.6	3	53.0	28.6	3
Ab–Ag association rate (k_+)	48.2	0.8	6	42.2	2.4	6
Administered Ab (Ab_0)	48.2	0.8	7	42.2	2.4	6
Biological clearance half-time of Ab (T_{bio})	47.9	0.2	8	41.2	0.0	8
Ab–Ag dissociation rate (k_-)	47.9	0.2	9	41.1	−0.2	9

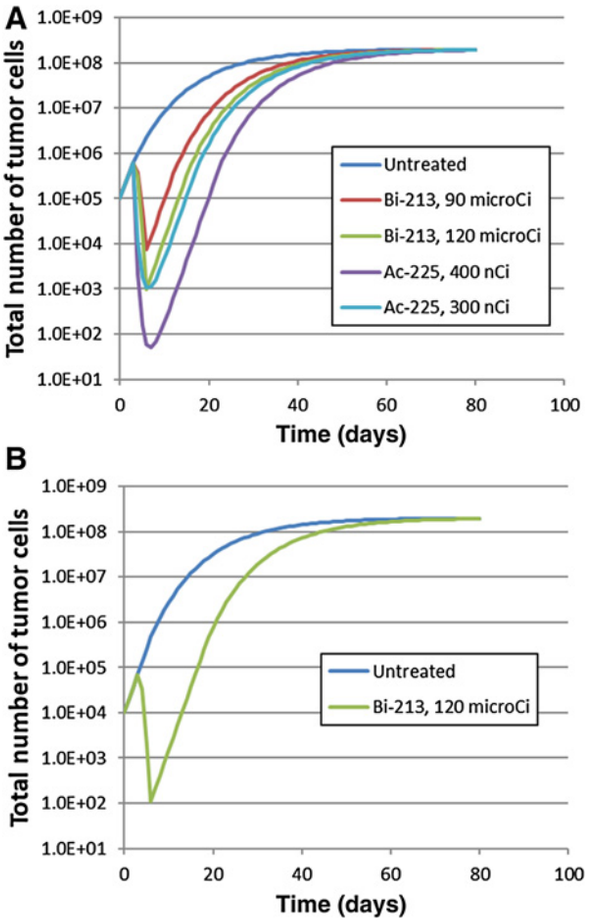

Figure 3.

Simulation-derived tumor cell number as a function of time post inoculation. The simulation was initiated on day 0 and treatment was simulated 3 days later. Simulations with an initial cell number of 10^5 NT2.5 untreated and treated with 120 or 90 μCi ^{213}Bi-labeled 7.16.4 or the same antibody labeled with 300 or 400 nCi ^{225}Ac (**A**) and 10^4 NT2.5 cells treated with 120 μCi ^{213}Bi-7.16.4 antibody (**B**). Median survival for each treatment simulation is taken as the day post tumor cell inoculation when the simulated cell number equals 10^8 cells.

administered constant but doubling specific activity (σ_0), doubling the number of antigen sites per cell (Ag_0), and the cell kill rate per unit absorbed dose, ($e = \frac{1}{D_0}$). The least impactful parameters relate to the amount of Ab administered (without increasing administered activity) and clearance kinetics ($k_+,\ Ab_0,\ T_{bio},\ k_-$). Corresponding results for ^{213}Bi-7.16.4 also showed that tumor doubling time and administered activity most impacted outcome but the magnitude of the percentage increase in survival was lower than that seen with ^{225}Ac. The increase in survival was also less sensitive to ^{213}Bi-7.16.4 delivery compared with the ^{225}Ac simulations; in contrast, the ^{213}Bi simulations were more sensitive to Ab–Ag association rate and amount of Ab administered.

Treatment fractionation simulations

Additional simulations were conducted to examine fractionated treatment. The 400 nCi single administration of ^{225}Ac-7.16.4 antibody was divided into two or four equal administrations. In every simulation, the first injection took place on day 3. The survival times for the treatment fractionation simulations are listed in Supplementary Table S1.

Figure 4A–H illustrates several important principles and provide some insight regarding the impact of fractionation on survival (as measured by the delay in reaching 10^8 cells). Aside from its impact on reducing toxicity (which is not specifically addressed in the current model), fractionation of RPT changes the treatment objective from "cure" to prolongation of survival. Cure requires reducing cell number to as close to zero as possible. Survival prolongation requires keeping the cell number below a threshold value for as long as possible. The fractionation scenarios depicted in **Fig. 4** show a survival prolongation but at the expense of depth of tumor cell kill. These observations are consistent with prior reports that have examined solid tumor targeting using radiation delivery (21, 30). **Figure 4A** shows that separating a 400-nCi administration into two, 200-nCi administrations, separated by 1 day leads to an approximate 25-fold reduction in tumor cell nadir compared with a single 400 nCi administration; this scenario also reduces median survival. In this case, the second injection is "wasted" because it is administered while the first is still in the circulation. **Figure 4B** and **E** show fractionation regimens in which the time-interval between injections leads to the same median survival as the single injection. This is explained by a subsequent administration that is given before the first has cleared (Supplementary Fig. S1).

Potential resistance to a fractionation regimen may become manifest if the first administration leads to a surviving tumor cell population that is either less sensitive to the alpha-emitter RPT or that exhibits a faster growth rate. We examine these scenarios in simulations in which the parameters associated with radiosensitivity or tumor growth rate are altered after the first administration so that the second and subsequent administrations encounter cells that differs from those of the first administration.

As would be expected, the results demonstrate that reduced radiosensitivity decreases the depth of the cell kill nadir. A 50% reduction in the rate of cell killing almost eliminates the survival prolongation advantage of fractionated RPT (Supplementary Fig. S2A–S2D). In the fractionated, 4-injection, 20-days-between-injection simulations (Supplementary Fig. S2D), the last two fractions cannot be administered because the number of cells has reached the 10^8 survival cutoff.

The survival cutoff is reached even sooner when, the first injection selects for a population of cells with a growth rate that is 50% greater than baseline (Supplementary Fig. S3A–S3D). In all cases, the 50% increase in growth rate leads to worse predicted biological outcome than a reduction in radiosensitivity. This is consistent with the high impact that tumor doubling time has on outcome (**Table 3**).

Discussion

We have developed a mathematical model that describes radiolabeled antibody targeting of rapidly accessible disseminated cancer cells. The model incorporates antibody pharmacokinetics, saturable antibody-antigen binding, and dissociation. Radiation-induced cell kiII and Gompertzian tumor cell growth are also modeled. The model was validated using preclinical studies in a disseminated breast cancer mouse model. Although the resulting model parameter values are specific to the particular breast cancer antibody–antigen pair and alpha-particle emitting radionuclide used in the preclinical studies, the resulting simulations are relevant to other saturable antigen-targeting antibodies with other alpha or beta-particle emitting radionuclides.

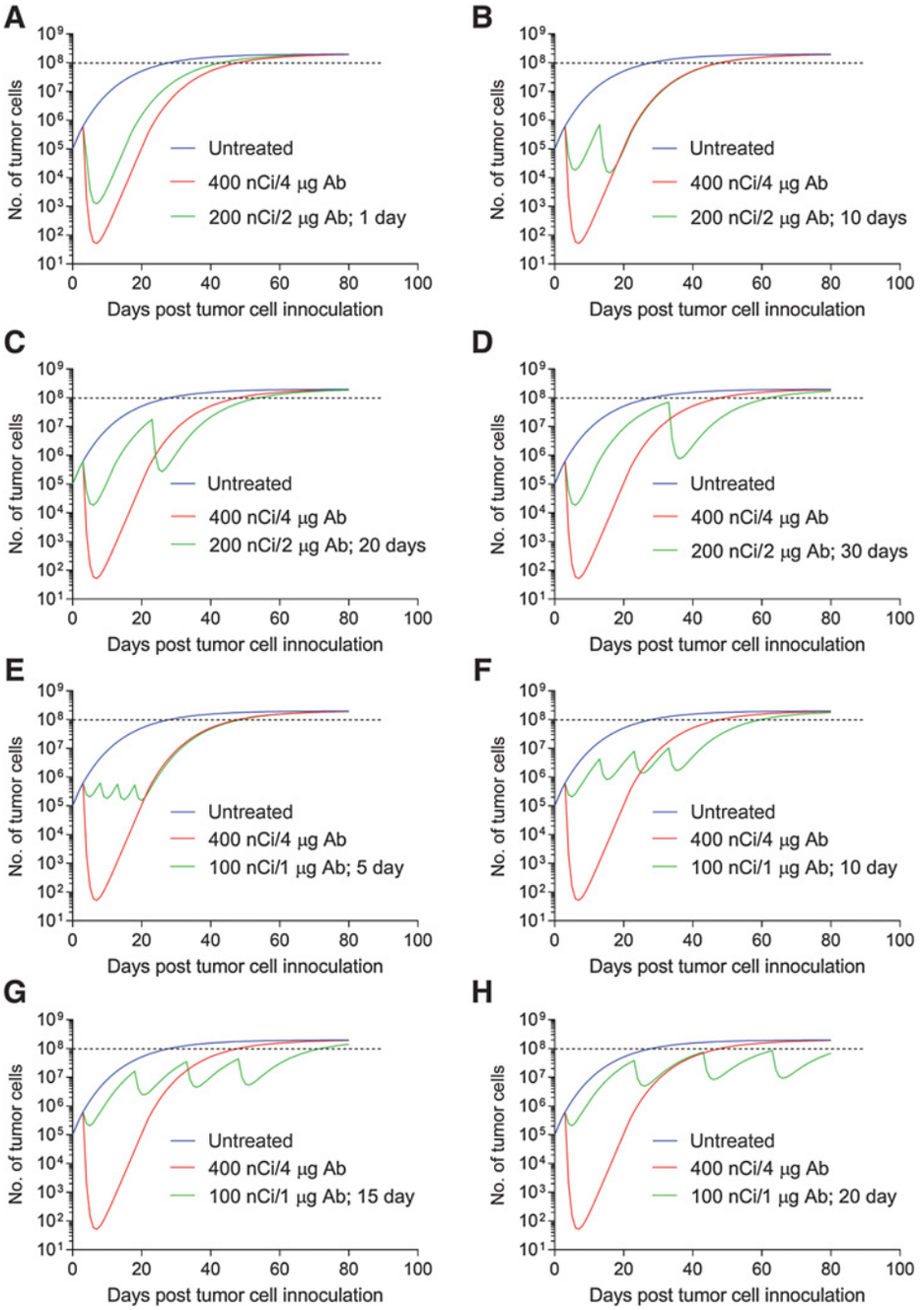

Figure 4.

Tumor cell number as a function of time post-tumor cell inoculation for two (**A–D**) or 4 (**E–H**) injections. A single, 400 nCi injection (red) was compared with no treatment (blue). Plots for two 200 nCi-injections, with the first one at 3 days and the second one at 1 (**A**), 10 (**B**), 20 (**C**), and 30 days (**D**) after the first are also shown. The 4-injection simulations had the second, third, and fourth 100 nCi injections separated by 5 (**E**), 10 (**F**), 15 (**G**), and 20 days (**H**). The tumor cell number that in untreated mice was reached on the same day postinoculation as median survival is indicated by the black dotted line.

Likewise, this model is also a starting point for simulating and optimizing human studies. The potential therapeutic benefit of RPT combined with agents that impact radiosensitivity or proliferation rate may also be examined using this model.

Our results show that the response model for antibody-mediated RPT predicts outcomes that are different from those observed for chemotherapy, wherein most agents clear rapidly from the circulation (either due to excretion or metabolism; ref. 31) and therapeutic effect depends on a high proliferation rate (32). In RPT, a high proliferation rate reduces efficacy and a shorter time-interval between agent administration does not necessarily improve survival.

The current model simulates survival, which may be more quickly obtained from preclinical studies especially when targeting metastatic cancer. Toxicity evaluations, including for example, hematologic parameters and liver and kidney function assays are beyond the scope of this work and would be best incorporated into the current model using data from human phase I studies.

Pharmacokinetic modeling of RPT has been previously used to understand antibody pharmacokinetics and tumor penetration (33), overcoming the barriers to radiolabeled antibody targeting (34), and also for treatment planning and to extract physiological parameters in patients using data from quantitative imaging (35–37).

We assume a single value for each of the parameters in the simulations presented in this work. It is unlikely that this is the case. Rather, one might expect that each of the single-valued parameters is actually a representative value of a distribution of values. We have shown previously that the results of a particular simulation will change if a parameter value is representative of a distribution (38). This is most impactful if the objective of modeling is outcome prediction. Because the model described in this work is founded on preclinical studies, the main objective of the work is to optimize treatment scenarios (e.g., fractionation schedules, combination with agents that affect tumor biology) that are most likely to succeed. Mathematical modeling can make predictions that can be experimentally tested, thus helping to confirm or reject the model. In this regard, mathematical modeling is not intended to replace experimentation but rather to reduce the scope of potential conditions that merit investigation and to provide a foundation for understanding the results of preclinical and clinical studies.

Disclosure of Potential Conflicts of Interest

No potential conflicts of interest were disclosed.

Authors' Contributions

Conception and design: A. Karimian, G. Sgouros
Development of methodology: A. Karimian, G. Sgouros
Acquisition of data (provided animals, acquired and managed patients, provided facilities, etc.): A. Karimian, N.T. Ji, H. Song
Analysis and interpretation of data (e.g., statistical analysis, biostatistics, computational analysis): A. Karimian, N.T. Ji, G. Sgouros
Writing, review, and/or revision of the manuscript: A. Karimian, N.T. Ji, G. Sgouros
Administrative, technical, or material support (i.e., reporting or organizing data, constructing databases): A. Karimian, G. Sgouros N.T. Ji
Study supervision: G. Sgouros

Acknowledgments

This work was supported by NIH grants R01CA116477 and R01CA187037.

The costs of publication of this article were defrayed in part by the payment of page charges. This article must therefore be hereby marked *advertisement* in accordance with 18 U.S.C. Section 1734 solely to indicate this fact.

Received September 6, 2019; revised October 30, 2019; accepted November 19, 2019; published first November 26, 2019.

References

1. Larson SM, Carrasquillo JA, Krohn KA, Brown JP, McGuffin RW, Ferens JM, et al. Localization of 131I-labeled p97-specific Fab fragments in human melanoma as a basis for radiotherapy. J Clin Invest 1983;72:2101–14.
2. De Jong M, Breeman WA, Bernard HF, Kooij PP, Slooter GD, Van Eijck CH, et al. Therapy of neuroendocrine tumors with radiolabeled somatostatin analogues. Q J Nucl Med 1999;43:356–66.
3. Wiseman GA, Kvols LK. Therapy of neuroendocine tumors with radiolabeled MIBG and somatostatin analogs. Semin Nucl Med 1995;25:272–8.
4. Houle S, Yip TK, Shepherd FA, Rotstein LE, Sniderman KW, Theis E, et al. Hepatocellular carcinoma: pilot trial of treatment with Y-90 microspheres. Radiology 1989;172:857–60.
5. Beierwaltes WH. Treatment of thyroid-carcinoma with radioactive iodine. Semin Nucl Med 1978;8:79–94.
6. Parker C, Nilsson S, Heinrich D, Helle SI, O'Sullivan JM, Fosså SD, et al. Alpha emitter radium-223 and survival in metastatic prostate cancer. N Engl J Med 2013;369:213–23.
7. Sgouros G, Allen BJ, Back T, Brill AB, Fisher DR, Hobbs RJ, et al. MIRD monograph: radiobiology and dosimetry for radiopharmaceutical therapy with alpha-particle emitters, Sgouros G, editor. Reston, VA: SNMMI; 2015.
8. Heskamp S, Hernandez R, Molkenboer-Kuenen JDM, Essler M, Bruchertseifer F, Morgenstern A, et al. α- versus β-emitting radionuclides for pretargeted radioimmunotherapy of carcinoembryonic antigen-expressing human colon cancer xenografts. J Nucl Med 2017;58:926–33.
9. Haro KJ, Scott AC, Scheinberg DA. Mechanisms of resistance to high and low linear energy transfer radiation in myeloid leukemia cells. Blood 2012;120:2087–97.
10. Rosenblat TL, McDevitt MR, Mulford DA, Pandit-Taskar N, Divgi CR, Panageas KS, et al. Sequential cytarabine and alpha-particle immunotherapy with bismuth-213-lintuzumab (HuM195) for acute myeloid leukemia. Clin Cancer Res 2010;16:5303–11.
11. Rosenblat TL, McDevitt MR, Pandit-Taskar N, Carrasquillo J. Phase I trial of the targeted alpha-particle nano-generator actinium-225 (Ac-225)-HuM195 (Anti-CD33) in acute myeloid leukemia (AML). Blood 2007;110:910.
12. Zalutsky MR, Reardon DA, Akabani G, Coleman RE, Friedman AH, Friedman HS, et al. Clinical experience with alpha-particle emitting 211At: treatment of recurrent brain tumor patients with 211At-labeled chimeric antitenascin monoclonal antibody 81C6. J Nucl Med 2008;49:30–8.
13. Nilsson S, Franzen L, Parker C, Tyrrell C, Blom R, Tennvall J, et al. Bone-targeted radium-223 in symptomatic, hormone-refractory prostate cancer: a randomised, multicentre, placebo-controlled phase II study. Lancet Oncol 2007;8:587–94.
14. Nilsson S, Parker C, Biggin C, Bruland O. Clinical experience and radiation safety of the first-in-class alpha-pharmaceutical, alpharadin (radium-223) in patients with castration-resistant prostate cancer (CRPC) and bone metastases. Int J Radiat Oncol Biol Phys 2010;78:S375–6.
15. Kratochwil C, Bruchertseifer F, Rathke H, Hohenfellner M, Giesel FL, Haberkorn U, et al. Targeted α-therapy of metastatic castration-resistant prostate cancer with (225)Ac-PSMA-617: swimmer-plot analysis suggests efficacy regarding duration of tumor control. J Nucl Med 2018;59:795–802.
16. Eisenhauer EA, Therasse P, Bogaerts J, Schwartz LH, Sargent D, Ford R, et al. New response evaluation criteria in solid tumours: revised RECIST guideline (version 1.1). Eur J Cancer 2009;45:228–47.
17. Wahl RL, Jacene H, Kasamon Y, Lodge MA. From RECIST to PERCIST: evolving considerations for PET response criteria in solid tumors. J Nucl Med 2009;50:122S.
18. Barendsen GW, Walter HMD, Bewley DK, Fowler JF. Effects of different ionizing radiations on human cells in tissue culture. III. Experiments with cyclotron-accelerated alpha-particles and deuterons. Radiat Res 1963;18:106–19.
19. Fowler JF. Radiobiological aspects of low dose rates in radioimmunotherapy. Int J Radiat Oncol Biol Phys 1990;18:1261–9.
20. Dale R, Carabe-Fernandez A. The radiobiology of conventional radiotherapy and its application to radionuclide therapy. Cancer Biother Radiopharm 2005;20:47–51.
21. O'Donoghue JA. The response of tumours with Gompertzian growth characteristics to fractionated radiotherapy. Int J Radiat Biol 1997;72:325–39.
22. Song H, Hobbs RF, Vajravelu R, Huso DL, Esaias C, Apostolidis C, et al. Radioimmunotherapy of breast cancer metastases with alpha-particle emitter 225Ac: comparing efficacy with 213Bi and 90Y. Cancer Res 2009;69:8941–8.
23. Song H, Shahverdi K, Huso DL, Wang Y, Fox JJ, Hobbs RF, et al. An immunotolerant HER-2/neu transgenic mouse model of metastatic breast cancer. Clin Cancer Res 2008;14:6116–24.
24. Song H, Shahverdi K, Huso DL, Esaias C, Fox J, Liedy A, et al. ^{213}Bi (alpha-emitter)-antibody targeting of breast cancer metastases in the neu-N transgenic mouse model. Cancer Res 2008;68:3873–80.
25. Reilly RT, Gottlieb MBC, Ercolini AM, Machiels JP, Kane CE, Okoye FI, et al. HER-2/neu is a tumor rejection target in tolerized HER-2/neu transgenic mice. Cancer Res 2000;60:3569–76.
26. Brechbiel MW, Pippin CG, McMury TJ, Milenic D, Roselli M, Colcher D, et al. An effective chelating agent for labeling of monoclonal antibody with 212Bi for alpha-particle mediated radioimmunotherapy. J Chem Soc Chem Commun 1991;17:1169–70.

27. McDevitt MR, Ma D, Simon J, Frank RK, Scheinberg DA. Design and synthesis of 225Ac radioimmunopharmaceuticals. Appl Radiat Isot 2002; 57:841–7.
28. Bast RC Jr, Kufe KW, Pollock RE. Chapter 38: Cytokinetics. In: Gilewski TA, Dang C, Surbone A, Norton L, et al., editors. Principles of chemotherapy. Holland-Frei cancer medicine. Hamilton, ON: BC Decker; 2000. p. 511–38.
29. Ballangrud AM, Yang WH, Palm S, Enmon R, Borchardt PE, Pellegrini VA, et al. Alpha-particle emitting atomic generator (Actinium-225)-labeled trastuzumab (Herceptin) targeting of breast cancer spheroids: efficacy versus HER2/neu expression. Clin Cancer Res 2004;10:4489–97.
30. O'Donoghue JA, Sgouros G, Divgi CR, Humm JL. Single-dose versus fractionated radioimmunotherapy: model comparisons for uniform tumor dosimetry. J Nucl Med 2000;41:538–47.
31. Powis G. Effect of human renal and hepatic disease on the pharmacokinetics of anticancer drugs. Cancer Treat Rev 1982;9:85–124.
32. Shackney SE, McCormack GW, Cuchural GJ Jr. Growth rate patterns of solid tumors and their relation to responsiveness to therapy: an analytical review. Ann Intern Med 1978;89:107–21.
33. Fujimori K, Fisher DR, Weinstein JN. Integrated microscopic-macroscopic pharmacology of monoclonal antibody radioconjugates: the radiation dose distribution. Cancer Res 1991;51:4821–7.
34. Sgouros G. Plasmapheresis in radioimmunotherapy of micrometastases: a mathematical modeling and dosimetrical analysis [see comments]. J Nucl Med 1992;33:2167–79.
35. Sgouros G, Graham MC, Divgi CR, Larson SM, Scheinberg DA. Modeling and dosimetry of monoclonal antibody M195 (anti-CD33) in acute myelogenous leukemia. J Nucl Med 1993;34:422–30.
36. Kletting P, Thieme A, Eberhardt N, Rinscheid A, D'Alessandria C, Allmann J, et al. Modeling and predicting tumor response in radioligand therapy. J Nucl Med 2019;60:65–70.
37. Hardiansyah D, Begum NJ, Kletting P, Mottaghy FM, Glatting G. Sensitivity analysis of a physiologically based pharmacokinetic model used for treatment planning in peptide receptor radionuclide therapy. Cancer Biother Radiopharm 2016;31:217–24.
38. Sgouros G, Song H. Cancer stem cell targeting using the alpha-particle emitter, 213Bi: mathematical modeling and feasibility analysis. Cancer Biother Radiopharm 2008;23:74–81.